Applied Geochemistry 146 (2022) 105439

Contents lists available at ScienceDirect

Applied Geochemistry

journal homepage: www.elsevier.com/locate/apgeochem

Feature

3D modelling of long-term sulfide corrosion of copper canisters in a spent nuclear fuel repository

Jin Ma [a,*], Marek Pekala [a,1], Peter Alt-Epping [a], Barbara Pastina [b], Susanna Maanoja [b,2], Paul Wersin [a]

[a] University of Bern, Institute of Geological Sciences, CH, 3012, Bern, Switzerland
[b] Posiva Oy, Finland

ARTICLE INFO

Editorial handling by: Dr Dmitrii A. Kulik

Keywords:
Radioactive waste disposal
Sulfide corrosion of copper canister
Microbial sulfate reduction
Reactive transport modelling
Long-term corrosion assessment

ABSTRACT

Copper canisters are a central component in the safety of the Finnish spent fuel repository concept (KBS-3), where the main corrodent potentially affecting the canister integrity is sulfide. In this study, a 3D numerical model is developed to assess the evolution of sulfide fluxes and the spatially resolved canister corrosion depths for the Finnish spent nuclear fuel repository concept. The backfilled tunnel and the disposal hole are implemented using repository geometries, with sulfide being produced at their interface with the rock (excavation damaged zone) by sulfate reducing bacteria (SRB). Recent experimental findings regarding the microbial sulfate reduction process as well as the scavenging of sulfide via iron (oxy)hydroxides are incorporated in the reactive transport model. Long-term simulations are performed, predicting a heterogeneous corrosion of the canister with a max. corrosion depth of 1.3 mm at the bottom corner after one million years. The evolution of sulfide fluxes shows two main phases, depending on the source of sulfate: first sulfate is supplied by the dissolution of gypsum from the bentonite barriers, followed by a steady, low-level supply from the groundwater. Sensitivity cases demonstrate that both the organic carbon and Fe(III) oxide contents in the bentonite are critical to the corrosion evolution, by being the main electron donor for SRB activities and the major sulfide scavenger in the bentonite, respectively. The backfilled tunnel contributes little to the flux of corrosive sulfide to the canister due to the attenuation by Fe(III)-oxides/hydroxides but induces a notable flux of sulfate into the disposal hole.

1. Introduction

The Finnish repository for spent nuclear fuel (SNF) at Olkiluoto is based on the KBS-3 disposal concept (Posiva, 2021). In this concept, multiple engineered barriers are designed to ensure the long-term safe storage of the spent nuclear fuel, including a copper-shielded metal canister and compacted bentonite materials surrounding the canister and backfilling the disposal tunnel (Fig. 1). The bentonite in the disposal tunnel, which lies above the disposal holes, is referred to as the backfill, while the bentonite around the canister in the disposal holes is referred to as the buffer (Fig. 1 (b)). The role of the bentonite barriers are essential, because they not only isolate the waste canister from the regional groundwater system by their extremely low permeability and favorable retention properties, but they also limit the transport of copper-corrosive agents towards the canister, among others. In anaerobic conditions, sulfide is the main species for copper corrosion in the repository environment (King et al., 2017), where it can be generated from sulfate by sulfate reducing bacteria (SRB). Although, in principal, the swelling of compacted bentonite after saturation with groundwater prevents microbial activity within itself, SRB can still be active in the excavation-damaged zones (EDZ) at rock/bentonite interfaces (Stroes-Gascoyne et al., 2010) and produce sulfide diffusing towards the copper canister. Experimental studies (Maanoja et al., 2020; Kiczka et al., 2021) have shown that bentonite can provide both sulfate and nutrients to SRB. On the other hand, bentonite may act as scavenger of sulfide (Svensson et al., 2017; Pedersen et al., 2017). For example, Fe (III) (oxy)hydroxides (termed Fe(III) oxides hereafter) present as accessory minerals in the bentonite may react with sulfide via a complex redox process (Poulton et al., 2004; Posiva, 2021) in which sulfide is immobilized via oxidation to sulfur and Fe(II) is released into the

* Corresponding author.
E-mail address: jin.ma@geo.unibe.ch (J. Ma).
[1] Currently at Federal Office for the Safety of Nuclear Waste Management (BASE), Germany.
[2] Currently at Tampere University, Materials science and environmental engineering unit, Finland.

https://doi.org/10.1016/j.apgeochem.2022.105439
Received 29 June 2022; Received in revised form 22 August 2022; Accepted 24 August 2022
Available online 30 August 2022

porewater. This Fe(II) may subsequently react with sulfide to form solid Fe-sulfide minerals such as mackinawite, thereby further attenuating the sulfide flux to the canister.

In recent years, the long-term copper corrosion due to sulfide has been studied by various numerical models (Smith et al., 2007; Stenlid et al., 2019; King et al., 2020). For instance, simple transport models assuming constant sulfide concentrations at the bentonite/host rock interface have been applied to estimate Cu corrosion depths (Briggs et al. (2016)), illustrating the important role of biogeochemical processes in regulating sulphide concentrations and fluxes in the host rock and the engineered clay barrier. One-dimensional reactive transport models have been developed to predict evolution of sulfide corrosion on copper canisters, accounting for the microbial reduction of sulfate in the repository using Monod kinetics (Cloet et al., 2017; Pekala et al., 2019a; King et al., 2020). Using a reactive transport model scheme and a simple 2D geometry, the impact of sulfide on Cu canister corrosion was assessed for the SNF repository at Olkiluoto (Wersin et al., 2014). This model was further extended to a 3D geometry of the near field and included Monod kinetics for describing microbial processes, (Wersin et al., 2017; Alt-Epping and Wersin, 2018a; Pekala et al., 2019b). By incorporating a realistic geometry of the repository into the model, it is now possible to accurately account for the distribution of materials and processes and for the length of transport pathways.

In this study, the newest development of the 3D reactive transport model for the assessment of sulfide in the Finnish SNF repository at Olkiluoto is described. It incorporates recent experimental findings regarding the microbial sulfate reduction process under site-specific conditions at Olkiluoto and the role of organic carbon as source for SRB activity in the bentonite barrier (Maanoja et al., 2020, 2021; Kiczka et al., 2021) as well as the scavenging of sulfide via Fe(III) oxides (Posiva, 2021). Long-term (up to one million years) simulations of sulfide fluxes and the heterogeneous corrosion of the copper canister are performed. The simulations include the dominant reaction processes controlling the corrosion rate of the canister: the dissolution of gypsum as the source of sulfate, the dissolution of organic matter as the dominant electron donor, and the attenuation of sulfide by reactive iron. The objective of this study is to assess the evolution of sulfide fluxes in the near field and its impact on copper canister corrosion using a realistic geometric representation of the repository and conservative but reasonable assumptions from current understanding regarding sulfide fluxes to the canister. The 3D reactive transport model focusses on the saturated anaerobic long-term evolution up to one million years and assumes constant ambient temperatures. The simulations provide space and time resolved estimates for the corrosion rate of the canister and hence enable predictions as to where and when the highest corrosion rate occurs. Although this 3D reactive transport model is rather complex compared to the ones used in the previous safety assessment, it should be born in mind that it represents an abstracted and simplified description of the biogeochemical system of a SNF repository. Therefore, the results of this study should not be interpreted as exact predictions, but rather estimations of the sulfide system on the pessimistic side. The simulations yield insights into the rate limiting processes controlling sulfide fluxes and the corrosion rate over a period of 1 million years. Furthermore, the contribution of the backfilled tunnel to sulfide corrosion is investigated, and the uncertainties in model conceptualization and parameterization is extensively discussed.

2. Conceptual biogeochemical model

The pathway of sulfide in the repository near field depends on the complex interplay between the sulfur, iron, carbon and hydrogen cycles (Pekala et al., 2019a). The main biogeochemical processes considered in the model are illustrated in Fig. 2. Since these processes may occur in different regions of the repository, the arrows in Fig. 2 may be seen as representing the transport of species between different regions.

2.1. Sulfide generation

Compacted bentonite is not suited to sustain the life of microbes. When emplaced at the target design density, the compacted bentonite will, once saturated, produce a high swelling pressure and a low free pore space, thus preventing microbial activity (Pedersen et al., 2000; Masurat et al., 2010; Stroes-Gascoyne et al., 2010; Stone et al., 2016). However, local damage to the rock caused during construction of the repository can result in enhanced porosity in the excavation-damaged zones (EDZ), the presence of which might trigger microbial activities.

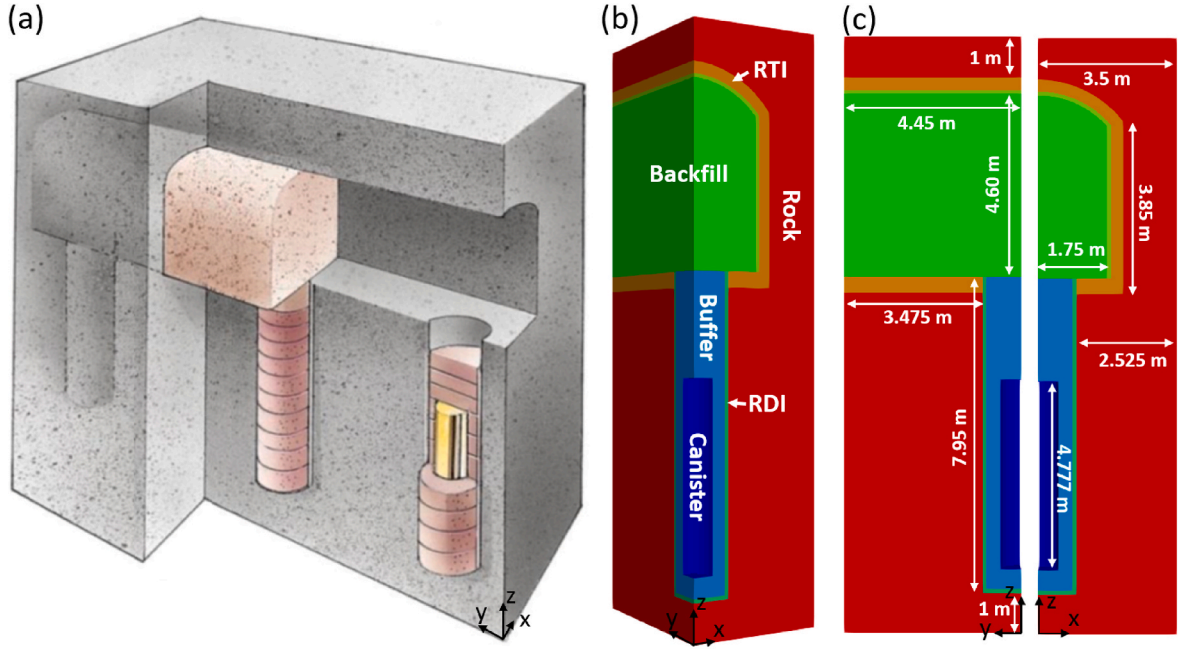

Fig. 1. (a) Sketch of the repository system. (b) Regions and materials within the model. RTI: rock tunnel interface; RDI: rock disposal hole (c) Dimensions of the model.

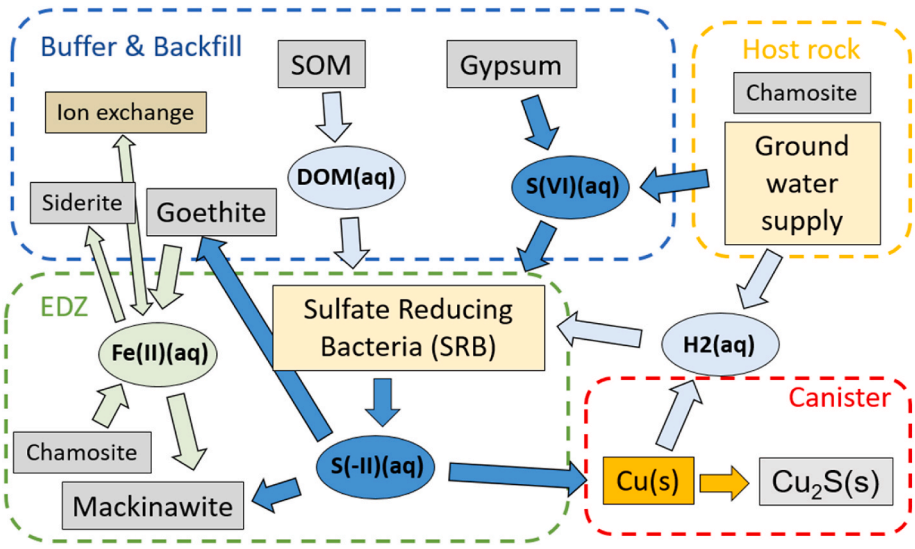

Fig. 2. Schematic of main processes considered in the conceptual biogeochemical model.

In this model, sulfate reducing bacteria (SRB), that can reduce dissolved sulfate (S(VI)) to sulfide (S(-II)) are assumed to be active exclusively in such excavation-damaged zones. Two SRB reactions are considered in the model, with different electron donors: dissolved organic matter (DOM) as shown in Eq. (1) (Wersin et al., 2011), or H_2(aq) as shown in Eq. (2) (Bagnoud et al., 2016).

$$2CH_2O(aq) + SO_4^{2-}(aq) \xrightarrow{SRB} \mathbf{HS^-(aq)} + H^+(aq) + 2HCO_3^-(aq) \quad (1)$$

$$4H_2(aq) + SO_4^{2-}(aq) + H^+(aq) \xrightarrow{SRB} \mathbf{HS^-(aq)} + 4H_2O \quad (2)$$

Note that CH_2O(aq) is used as a simplified stoichiometric formula representing DOM with an average carbon oxidation number of zero. In Eq. (1) the release of CO_2 is the source for acidity, while Eq. (2) produces alkalinity.

SRB activity is represented using a Monod kinetics model:

$$R_{SRB}^{DOM} = k_{max}^{DOM} \cdot \left(\frac{[DOM]}{[DOM] + K_{DOM}^{S}}\right) \cdot \left(\frac{[SO_4^{2-}]}{[SO_4^{2-}] + K_{SO_4^{2-}}^{S}}\right) \quad (3)$$

$$R_{SRB}^{H_2} = k_{max}^{H_2} \cdot \left(\frac{[H_2]}{[H_2] + K_{H_2}^{S}}\right) \cdot \left(\frac{[SO_4^{2-}]}{[SO_4^{2-}] + K_{SO_4^{2-}}^{S}}\right) \quad (4)$$

where R^{DOM}_{SRB} and R^{H2}_{SRB} are the sulfate reduction rates considering DOM and hydrogen as the electron donor, respectively, [DOM], [H_2], [SO^{2-}_4], and [HS^-] are the concentrations of DOM and dissolved hydrogen, and the activities of sulfate and sulfide, respectively, k^{DOM}_{max} and k^{H2}_{max} are the maximum rate constants for DOM and hydrogen as the electron donor, respectively, and K^{S}_{H2} and K^{S}_{SO42-} are the half-saturation constants for hydrogen and sulfate, respectively (refer to Section 3.4 for parameter values).

The total sulfate reduction rate (R^{TOTAL}_{SRB}) can be expressed by the sum of the sulfate consumed by the two electron donor pathways:

$$R_{SRB}^{TOTAL} = -\frac{d[SO_4^{2-}]}{dt} = \frac{d[HS^-]}{dt} = R_{SRB}^{DOM} + R_{SRB}^{H_2} \quad (5)$$

2.1.1. Sources of electron donors

DOM is released by solid organic matter (SOM) from the bentonite in the backfill and the buffer:

$$SOM(s) \rightarrow DOM(aq) \quad (6)$$

The dissolution of SOM is represented as a kinetic reaction of the form:

$$R_{SOM} = k_{SOM} \cdot \left(1 - \frac{[DOM]}{[DOM_{max}]}\right) \quad (7)$$

where R_{SOM} is the SOM dissolution rate, k_{SOM} is the rate constant of SOM dissolution, [DOM] is the DOM concentration, and [DOM_{max}] is the maximum DOM concentration (refer to Section 3.4 for parameter values).

H_2(aq) in the system is continuously supplied by the copper corrosion reaction (Eq. (13)), as well as by the dissolved H_2 in groundwater (emanating from the rock). Other than the reaction with SO_4^{2-} (Eq. (2)), H_2 is assumed to be inert, thus exerting no control on Eh.

2.1.2. Sources of sulfate

Gypsum ($CaSO_4 \cdot 2H_2O$), that is initially present in the backfill and buffer, serves as the major source of sulfate in early times.

$$CaSO_4 \cdot 2H_2O(s) \leftrightarrow Ca^{2+}(aq) + \mathbf{SO_4^{2-}(aq)} + 2H_2O \quad (8)$$

After the depletion of gypsum in the near field, groundwater in the host rock continues to provide sulfate to the system.

2.2. Sulfide attenuation: iron system

During the transport of sulfide, dissolved Fe and Fe-minerals act as efficient scavengers for sulfide in anaerobic environments (Pekala et al., 2019a; Rickard and Luther, 2007). Fe(III) minerals, such as goethite, present as accessory mineral in the backfill and buffer, can react with sulfide directly and release aqueous Fe(II) (for details, refer to Supplementary Information (SI)-Section 3):

$$2FeOOH(s) + HS^-(aq) + 5H^+ \rightarrow 2Fe^{2+}(aq) + S^0 + 4H_2O \quad (9)$$

It should be noted that the sulfidation of Fe(III) oxides involves a complex redox reaction with a number of intermediate steps (e.g. Dos Santos Afonso and Stumm, 1992; Poulton et al., 2004). These are not explicitly accounted for in the model and a simplified kinetic rate based on experimental data is considered for the reaction. For simplicity, the formation of elemental sulfur in Eq. (9) is not explicitly considered in the model, so that sulfide reacting with Fe(III) oxides is removed irreversibly from the system.

Furthermore, sulfide can be also consumed by iron sulfide (mackinawite) precipitation via Fe(II) produced partially by the sulfidation reaction (Eq. (9)):

$$Fe^{2+}(aq) + HS^-(aq) \leftrightarrow FeS(s) + H^+(aq) \quad (10)$$

Due to the lack of data and to be on the conservative side, further transformation from mackinawite to more insoluble pyrite is not considered in this model.

Aside from Fe(II) released from goethite, aqueous Fe(II) is initially present in the pore waters in the model, and will be continuously supplied by the groundwater in the host rock. The Fe concentration in the groundwater is controlled by Fe-bearing minerals in the rock, such as biotite or chlorite. Here we assume that only chlorite (chamosite) is present in the EDZ and the host rock:

$$Fe_5Al(AlSi_3)O_{10}(OH)_8 + 16H^+ \rightarrow 5Fe^{2+} + 2Al^{3+} + 3H_4SiO_4 + 6H_2O \quad (11)$$

Cation exchange reactions (Section 2.4) and the precipitation of Fe (II)-bearing minerals such as mackinawite (Eq. (10)) and siderite (Eq. (12)) also affect the Fe concentration in the system.

$$Fe^{2+}(aq) + CO_3^{2-}(aq) \leftrightarrow FeCO_3(s) \quad (12)$$

2.3. Corrosion of the copper canister

A fraction of the sulfide eventually diffuses through the bentonite, and can reach the canister surface, where it instantly reacts with metallic copper to produce chalcocite (Cu_2S):

$$2Cu(s) + HS^-(aq) + H^+(aq) \rightarrow Cu_2S(s) + H_2(aq) \quad (13)$$

The corrosion reaction is considered to be limited by the sulfide flux to the canister. Therefore, canister corrosion depth is proportional to the time-integrated sulfide flux. The description assumes a general corrosion mode and is compatible with the corrosion model put forward by King et al. (2017). Hydrogen generated by Eq. (13) can diffuse back towards the interface areas, where it is utilized by SRB (Eq. (2)) as indicated by Fig. 2.

2.4. pH buffering and cation exchange reactions

Sulfate reduction in the interface areas affects alkalinity and pH (Eq. (1) and (2)). In the bentonite, changes in pH are resisted by goethite dissolution (Eq. (9)) and calcite equilibrium reactions:

$$CaCO_3(s) + H^+(aq) \leftrightarrow Ca^{2+}(aq) + HCO_3^-(aq) \quad (14)$$

Furthermore, pH in the bentonite is buffered due to surface protonation reactions occurring on the edge surfaces of abundant montmorillonite:

$$\equiv SOH \leftrightarrow \equiv SO^- + H^+(aq) \quad (15)$$

$$\equiv SOH + H^+(aq) \leftrightarrow \equiv SOH_2^+ \quad (16)$$

In the interface areas and in the intact rock, pH decrease is additionally resisted by kinetic dissolution of silicates such as chlorite and kaolinite (Eq. (11)).

In the buffer and backfill, major cations (Na^+, Ca^{2+}, Mg^{2+}, K^+, Fe^{2+}) undergo equilibrium exchange reactions according to:

$$\frac{1}{i}I^{i+} + \frac{1}{j}JX_j \leftrightarrow \frac{1}{i}IX_i + \frac{1}{j}J^{j+} \quad (17)$$

where X is the exchange site, J is reference cation, and I is exchanging cation.

3. Model description

3.1. Model geometry

A 3D reactive transport model is developed using PFLOTRAN (www.pflotran.org) with the adapted Thermochimie thermodynamic database v.9.0b. The model geometry follows the Finnish multi-barrier KBS-3V concept (Salonen et al., 2021; Wersin et al., 2017), in which copper-iron canisters are emplaced vertically in individual disposal holes and surrounded by swelling bentonite, as shown in Fig. 1(a). Intact crystalline host rock adjacent to the backfill and buffer is presented with the distinct properties from the bulk host rock. The EDZ is assumed to extend 10 cm around the disposal hole (rock disposal hole interface, RDI), 40 cm under the tunnel and 30 cm around the walls and ceiling of the tunnel (rock tunnel interface, RTI) (Pekala et al., 2019a).

The spacing between the cylindrical disposal holes (at the center) is 8.9 m. Due to intrinsic symmetries (groundwater flow is not considered), the geometry of the model can be reduced to a quarter of the repository unit with a tunnel length of 4.45 m. The model geometry (quarter geometry) is presented in Fig. 2(b and c), where the host rock compartment extends 1 m away from the top of the tunnel and below the disposal hole, and 1.35 m away from the side tunnel wall.

3.2. Material properties

Different materials are used for the defined regions. The physical properties of the materials are listed in Table 1, the mineral compositions are listed in Table 2, and more details in SI-Section 2. The inside of the canister is considered inactive, thus only the surface of the canister are represented, where Eq. (13) takes place.

3.2.1. Buffer

The reference material in the model for the buffer is a Na-rich Wyoming bentonite. The buffer material has a dry bulk density of 1557 kg/m^3, a porosity of 0.43, and an effective diffusion coefficient of $2{\cdot}10^{-11}$ m^2/s (Wersin et al., 2014; Posiva, 2021).

The main mineral in the Wyoming bentonite is smectite (montmorillonite), amounting to about 83 wt% (Kiviranta et al., 2018). Accessory minerals, such as quartz, illite, calcite, feldspar, gypsum, and Fe oxides (goethite) are identified by X-ray diffraction analysis (XRD) (Kiviranta et al., 2018). The content of organic carbon (i.e., SOM), together with inorganic carbon, sulfate, and sulfide, are determined using LECO chemical analysis (Karnland et al., 2006; Kiviranta et al., 2018). The latter values are then used to quantify the content of calcite, gypsum, and pyrite. The amount of iron oxides is generally low and difficult to estimate from XRD analysis. Bradbury and Baeyens (2002) determined the amount of "total iron (hydr)oxide" by dithionite-citrate-bicarbonate extraction procedure on bulk Wyoming bentonite to be 25.9 ± 0.7 mmol/kg, which corresponds to 0.23 wt% of goethite (FeOOH). For simplicity, smectite is considered inert and only reactive minerals are included in the buffer, as listed in Table 2.

Montmorillonite sorption properties are calculated based on Posiva (2021). Cation exchange and surface protonation model parameters are taken from Bradbury and Baeyens (2003), and Bradbury and Baeyens (1997), respectively. In addition, Fe exchange is included in the model for buffer and backfill with selectivity coefficients reported by Charlet and Tournassat (2005).

3.2.2. Backfill

The backfill material is Italian bentonite. The material has a dry bulk density of 1425 kg/m^3 and a porosity of 0.502 (Kiviranta et al., 2018). The effective diffusion coefficient of the backfill is estimated according to the empirical D_e-dry density relationship proposed by Kiczka et al.

Table 1
Porosities (φ) and effective diffusion coefficients (De) used for the buffer, backfill, interface areas (RTI & RDI), and the intact rock.

	φ [%]	De [m^2/s]
Buffer	43	2.0×10^{-11}
Backfill	50.2	2.7×10^{-11}
RTI	1	5.0×10^{-13}
RDI	2	1.5×10^{-12}
Rock	0.515	2.0×10^{-13}

Table 2
Initial geochemical conditions. (1) 1 mg C/L_{water} of organic carbon assuming molar mass of pure carbon (12 g/mol), (2) 2 mg C/L_{water} of organic carbon assuming molar mass of pure carbon (12 g/mol), (3) a trace amount of kaolinite assumed to be present in the buffer and backfill (0.1 wt%), and in the rock (0.001 wt%) (†) secondary minerals (allowed to form if over-saturated).

	Rock & EDZ	Buffer	Backfill
pH	7.12	7.65	7.64
pe	−3.25	−3.14	−4.07
Eh (mV)	−192	−0.19	−0.24
Total component [mol/L_{water}]			
Al	2.77E-09	8.72E-09	8.75E-09
C(4)	1.70E-03	1.16E-03	1.39E-03
Ca	1.62E-02	1.15E-02	1.20E-02
Cl	1.14E-01	4.85E-02	1.02E-01
Fe	1.82E-05	2.21E-06	2.98E-06
K	4.90E-04	5.34E-04	7.76E-04
Mg	7.46E-03	5.32E-03	2.88E-02
Na	7.71E-02	1.32E-01	1.85E-01
S(-II)	6.28E-07	2.41E-07	3.24E-07
S(VI)	4.82E-03	5.85E-02	8.21E-02
Si	1.82E-04	1.82E-04	1.81E-04
DOM	(1)8.33E-05	(2)1.67E-04	(2)1.67E-04
H_2(aq)	1.00E-03	1.00E-03	1.00E-03
Reactive minerals [wt.%]			
Gypsum	(†)0.00	1.07	1.2E-01
Calcite	1.0E-03	8.3E-01	2.42
Quartz	9.64	3.80	4.0E-01
SOM	0.00	2.3E-01	3.4E-01
Goethite	(†)0.00	2.3E-01	1.30
(3)Kaolinite	1.0E-03	1.0E-01	1.0E-01
Chlorite	4.7E-03	(†)0.00	(†)0.00
Siderite	(†)0.00	(†)0.00	(†)0.00
Mackinawite	(†)0.00	(†)0.00	(†)0.00
Surfaces [mol/L_{water}]			
S_{w1}	NA	0.119	0.102
S_{w2}	NA	0.119	0.102
Exchanger [eq/L_{water}]			
CEC	NA	3.367	3.035

(2020), as $2.7{\cdot}10^{-11}$ m^2/s.

Like in the Wyoming bentonite, smectite composes the majority (about 83 wt%) of the Italian backfill bentonite (Kiviranta et al., 2018; Posiva, 2021). Accessory minerals, such as quartz, illite, calcite, feldspar, and Fe oxides (mostly hematite) are identified from XRD data. Note that for simplicity, Fe oxides are represented by goethite as in the buffer. The LECO chemical analysis (Karnland et al., 2006) yields about 0.34 wt % SOM, but very low content of sulfur (thus low amounts of gypsum and pyrite). The reactive backfill mineral composition is listed in Table 2.

3.2.3. Host rock and EDZ

The granitic host rock at Olkiluoto is fractured and fractures are coated with clay minerals (kaolinite, illite), Fe-sulfides (pyrrhotite and pyrite), calcite, and chlorite (Aaltonen et al., 2018). The rock matrix mostly comprises high-grade metamorphic gneisses, containing quartz, feldspars, and mica. As a simplification, the fractured rock is treated as homogeneous porous medium in the model, in which only kaolinite, calcite, chlorite, and quartz are considered as active minerals in the rock (Table 2). The content of chlorite (chamosite) is estimated based on the fracture density and coating thickness (Fox et al., 2012; Aaltonen et al., 2018) (for details, see SI-Section 1), whereas arbitrary contents of quartz, calcite, and kaolinite are implemented in the host rock. The rock porosity of 0.515% is adopted from Pekala et al. (2019a), which is estimated based on Hartley et al. (2013). The value of the effective diffusion coefficient of the rock is also adopted from Pekala et al. (2019a) (Table 1).

For the interface areas (RTI and RDI), the same mineral compositions as the host rock are considered. The physical porosities are taken after Hartley et al. (2013), and the effective diffusion coefficients are adopted from Pekala at al. (2019a) (Table 1).

3.3. Boundary and initial conditions

3.3.1. Boundary conditions

The three vertical faces (at x = 0 m, y = 0 m, and y = 4.45 m) of the model are considered closed due to symmetry (Fig. 2), whereas the top face (z = 14.95 m), bottom face (z = 0 m), and one side face (x = 3.5 m) are open. The initial pore water is at hydrostatic pressure with fixed top boundary pressure of 4.5 MPa, and isothermal condition with a uniform temperature of 25 $^{\circ}C$ are assumed. In such settings, we expect that only diffusive transport occurs across these open boundaries. The water chemistry at the open boundaries is identical to the initial groundwater in the rock, as listed in Table 2.

3.3.2. Initial pore water compositions

The evolution of the composition of the groundwater at repository depths is not known with certainty as it may change over a million years due to climate variations and changes in subsurface hydrology. In this study, we assume that the groundwater has a composition corresponding to the sulfate-rich brackish groundwater throughout the assessment period. This is a conservative assumption regarding sulfide fluxes as the brackish water is characterised by the highest concentration of dissolved sulfate ($4.82{\cdot}10^{-3}$ mol/L or ca. 460 mg/L) of all reference and bounding groundwater types defined in Hellä et al. (2014). DOM concentration in the groundwater is assumed to be 1 mg C/L, based on measurements in the Olkiluoto groundwater (Mäkelä et al., 2016), and the concentration of dissolved hydrogen is assumed to be 10^{-3} mol/L. The initial composition of the groundwater is listed in Table 2 (Rock and Interface areas). The same composition is used as a fixed (Dirichlet) boundary condition for transport along the open boundaries.

The initial compositions bentonite porewaters (as listed in Table 2) were modelled based on the approach described in Wersin et al. (2016) and assuming mixing of residual water and groundwater (SI-Section 2). Based on Kiczka et al. (2021), the concentration of DOM present in the bentonite porewater is estimated to be 2 mg C/L. This assumption may be conservative as the value, used to represent SOM solubility in the bentonite over a period of a million years, was calibrated from short term laboratory experiments, during which the solubility may be over-estimated due to leaching of soluble components over time.

Initial H_2(aq) concentration in the buffer and backfill porewaters are assumed to equal the concentrations in the groundwater, 10^{-3} mol/L, considering that H_2(aq) is supplied to the bentonite porewater during its saturation with the groundwater and that there is no source or sink of H_2(aq) within the buffer/backfill.

3.4. Reaction rate implementation

The SRB reactions are represented by the standard Monod formulation, where single lumped rate constants ($k^{DOM}{}_{max}$ and $k^{H2}{}_{max}$ in Eqs. (1) and (2), respectively) are used. Such simplified formulation implies that: (i) potential changes in bacterial population size in time and space are disregarded, (ii) the availability of other constituents (such as P or N) required to sustain SRB activity are never limiting, and (iii) at full availability of DOM/H_2(aq) and dissolved sulfate the reaction proceeds at maximum rate defined by the lumped rate constant. Based on sulfide production rates derived from field and laboratory studies (Goldhaber and Kaplan, 1975; Richards and Pallud, 2016, and references within), the value of this rate constant (i.e. the maximum sulfide production rate assuming full availability of reaction substrates), for the DOM and H_2(aq) pathways, is defined at $5{\cdot}10^{-5}$ and 10^{-4} $mol_{sulfide}/(L_{water}{\bullet}year)$, respectively. In addition, the value of $K_{SO4} = 10^{-5}$ [mol/L] (Nethe--Jaenchen and Thauer, 1984) is used, while for K_{DOM} the value $5{\cdot}10^{-6}$ [mol/L] is used (corresponding to that of acetate when used as reductant – Jin et al., 2013). The reported values of K_{H2} are between $1.3{\cdot}10^{-6}$ and $20{\cdot}10^{-6}$ [mol/L] (Maia et al., 2016) and a value of $4{\cdot}10^{-6}$ [mol/L] is adopted (Table 3).

At the canister surface, sulfide is consumed by a fast kinetic reaction

Table 3
Rate constants and surface areas (or microbe densities) for the mineral (or microbial) reactions. * Microbial reactions using the Monod formulation.

Mineral	Reaction	Rate constant	Surface area	Rate dependency
Kinetic reaction:		[mol/m^2/s]	[m^2/m^3]	
SOM	Eq. (6)	1.0×10^{-6}	1.0	
Gypsum	Eq. (8)	1.0×10^{-6}	1.0	
Goethite	Eq. (9)	1.75×10^{-3}	14.0 [m^2/g]	HS^- and H^+ (first order)
Mackinawite	Eq. (10)	1.0×10^{-9}	1.0	
Chlorite	Eq. (11)	6.4×10^{-17}	0.36	H^+
Siderite	Eq. (12)	1.0×10^{-6}	1.0	
Calcite	Eq. (14)	1.0×10^{-6}	1.0	
Quartz		1.0×10^{-6}	1.0	
Kaolinite		1.0×10^{-6}	1.0	
Microbial reactions:*		[mol/L$_w$/s]	Biomass [mol/m^3]	Monod rate constant [mol/L]
SRB	Eq. (1)	1.6×10^{-12}	1.0	$K_{DOM} = 5 \times 10^{-6}$, $K_{SO4} = 10^{-5}$
	Eq. (2)	3.2×10^{-12}	1.0	$K_{H2} = 4 \times 10^{-6}$, $K_{SO4} = 10^{-5}$
Copper	Eq. (13)	1.0×10^{-6}	N/A	$K_{HS} = 10^{-15}$

mimicking the formation of chalcocite (Cu_2S). The corrosion reaction is assumed to be instantaneous, such that the corrosion rate is controlled by the rate of sulfide mass transport towards the canister surface. Except for copper, all the other minerals' dissolution and precipitation rates are calculated based on transition state theory. Recent experiments on bentonites (Kiczka et al., 2020; Maanoja et al., 2020, 2021) show that organic matter (possibly retained by sorption onto montmorillonite surfaces) may be released from the bentonite into the porewater almost instantly. Therefore, an arbitrary fast SOM dissolution rate is used in the model to establish local equilibrium (i.e. a max. DOM concentration of 2 mg/L). Besides SOM, arbitrary fast reaction rate constants are also used to impose local equilibrium for gypsum, calcite, siderite, quartz, and kaolinite.

We use goethite as a proxy for Fe(III) oxide minerals undergoing sulfidation reactions. Goethite sulfidation (Eq. (9)) is assumed to proceed via a kinetic reaction with first order kinetics in sulfide and hydrogen ion concentrations (details refer to SI-Section 3). The kinetics of goethite sulfidation is associated with some uncertainty. Here we attempt to use a high rate constant, a high reactive surface area of 14 m^2/g (Dos Santos Afonso and Stumm, 1992) and include the activities of HS^- and H^+ in the rate equation (SI Eq. A-8) such that the effective dissolution rate of goethite is limited by the supply of the sulfide and/or hydrogen ions (i.e. the pH). Note that, compared to experimental results, a reduced goethite dissolution rate is used in the calculations to facilitate better numerical performance with a conservative model assumption (detailed in SI-Section 3).

3.5. Calculation of canister corrosion depth

Two types of corrosion depths at the canister surface are calculated: the surface-averaged corrosion depth, and the cell-resolved corrosion depth. The surface-averaged corrosion depth (d_{avg}) reflects the time-integrated sulfide flux to the canister, calculated as:

$$d_{avg} = \frac{2 \times \sum_S M_{HS^-} \times V_{m,\,Cu}}{S_{can}} \tag{18}$$

where $\sum_S M_{HS^-}$ is the sum of the total sulfide that reaches the canister surface (mol), $V_{m,\,Cu}$ is the molar volume of copper (m^3/mol), and S_{can} is the total surface area of the canister (m^2). The surface-averaged corrosion rate provides limited information as to the risk of canister failure and is used here as a parameter to assess and compare the temporal evolution of corrosion under different model assumptions.

Like the other parts of the model, the canister surface is meshed into cells, and cell-resolved corrosion depths (d_{cell}) are calculated in each cell. Although cell resolved corrosion depths are integrated over the area of the cell interfacing the buffer, these provide a space resolved and much more accurate assessment of the risk of canister failure. In order to capture more details near the top and bottom of the canister, a non-uniform vertical discretization is used, with the finest cells (1 cm in height) at the top and bottom corner of the canister and larger cells in the middle of the canister. The cell-resolved corrosion depths depend on the cell size of the canister surface, and are calculated as below:

$$d_{cell} = \frac{2 \times M_{HS^-} \times V_{m,\,Cu}}{S_{cell}} \tag{19}$$

where M_{HS^-} is the moles of sulfide that reaches the cell (mol), and S_{cell} is the surface area of that cell interfacing the buffer (m^2).

4. Results

4.1. General evolution

The evolution of the system in the near field depends on the complex interplay among the sulfur, iron, and carbon/hydrogen cycles which are to a large extent driven by the reactivity and availability of primary and the formation of secondary solid phases (Fig. 3). In general, the global evolution of the system was found to display two phases based on the simulation results discussed in detail in the following Sections 4.2-4.4:

Phase I: Up to ca. 300 ky, when the rate of sulfide production is controlled by both DOM transport and the maximum sulfide production rate (Table 3), with excess sulfate in the near field system. During this phase, sulfate is supplied by the initial sulfate in the porewater and dissolution of gypsum in the backfill and buffer (Fig. 3). In fact, there is so much sulfate in the system that it diffuses outwards across the open boundaries (Fig. 4(a)). The model predicts depletion of gypsum after about 190 ky (Fig. 3), which is a key driver for the transition from Phase I to Phase II.

Phase II: From ca. 300 ky to 1 My, when sulfate is mostly supplied by groundwater via inward-diffusion from the open boundaries (Fig. 4(a)). During this phase, sulfide production is strongly limited by the transport of sulfate from groundwater. Following the depletion of goethite around the canister at about 400 ky, a more or less stable flux of sulfide towards the canister is established at about $3 \cdot 10^{-5}$ mol/(m^2·y).

4.2. Sulfide production

The production rate of sulfide is controlled by the concentration of dissolved sulfate, DOM and H_2 in the EDZ, as decribed in Eqs. (3) and (4). Sulfate is in excess during Phase I, and becomes rate-limiting in Phase II. SOM is predicted to be depleted only in the very long term (towards 1 My), and exclusively at the bottom of the buffer (Fig. 3). Therefore, with the assumed fast SOM dissolution rate, DOM in the clay is largely present nearly at the maximum SOM solubility (2 mg C/L) throughout the calculation. The initial H_2(aq) contributes to the early peak of the sulfide flux (Fig. 4(b)). However, H_2(aq) in the buffer is consumed within the first 100 years, and for the rest of the simulation, H_2(aq) is mainly supplied by diffusion from the surrounding groundwater and corrosion of the canister (Eq. (13)). As shown in Fig. 4(c), the concentration of DOM is about 3–4 orders of magnitude higher than that of H_2 in the RDI after about 500 y. Therefore, the overall sulfide production is strongly dominated by the DOM pathway after 500 y. At 1 My, the DOM pathway has contributed to 94% of total produced sulfide (5211 mol), while the H_2(aq) pathway accounts for only 6% (Fig. 4(d)). The total sulfide production rate reaches 82.4 mmol/y in the first year, due to high initial concentration of sulfate and H_2 in the pore waters.

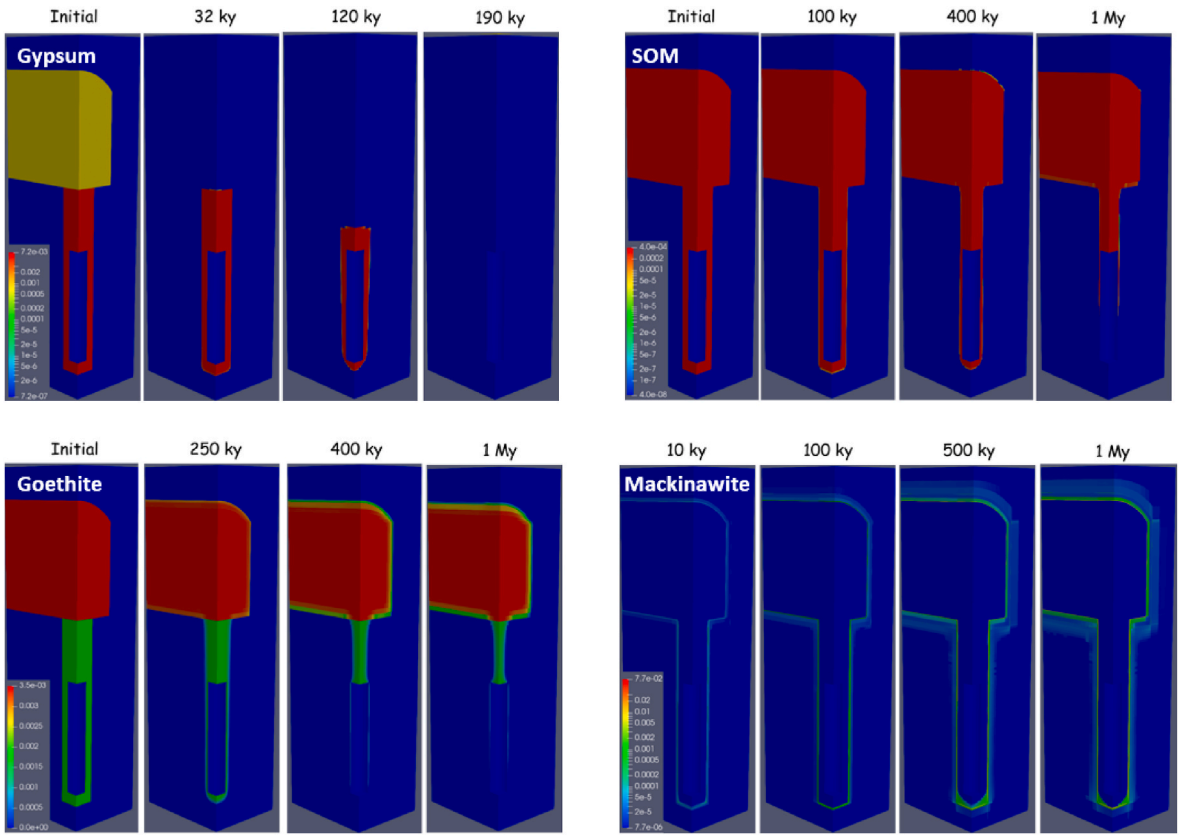

Fig. 3. Evolution and distribution of major solid phases (gypsum, SOM, goethite and mackinawite) in the whole modelat selected times.

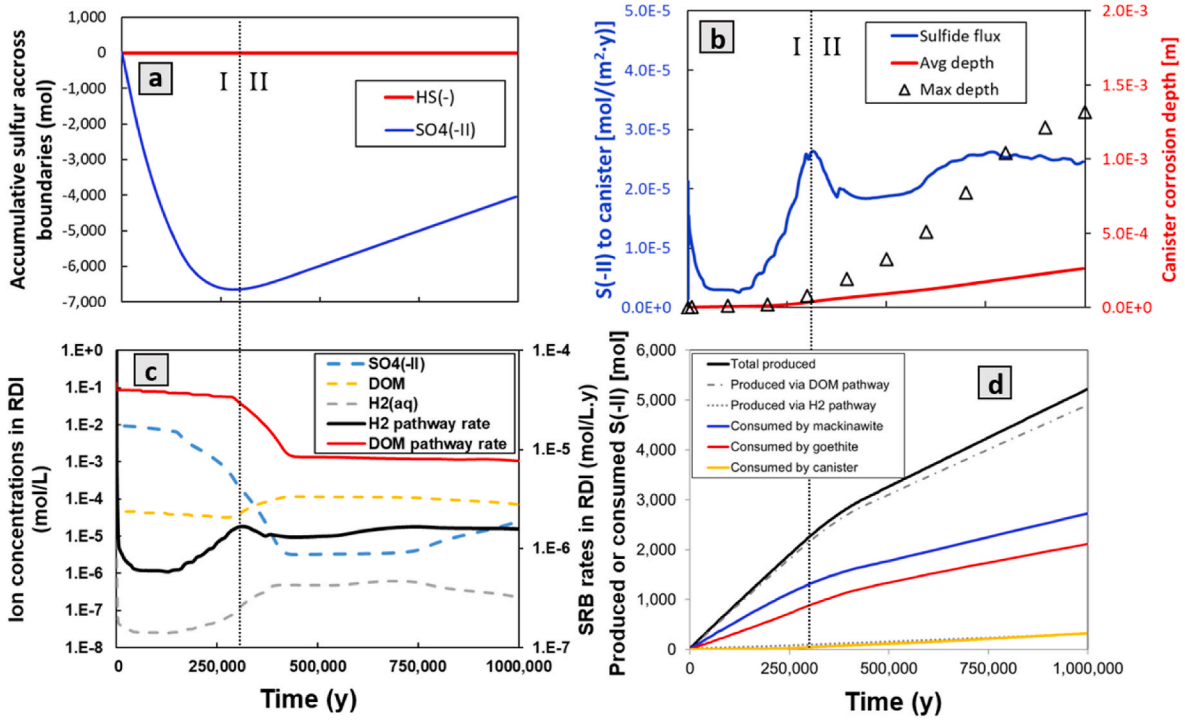

Fig. 4. Evolution of the sulfide system in two distinctive phases (I and II). (a) The amount of HS^- and $SO4^{2-}$ diffusing into (positive) or out of (negative) the system through boundaries. (b) Sulfide fluxes to the canister surface (blue line), the surface-averaged corrosion depth (red line) and the max. cell-resolved corrosion depth (black triangles) of the canister. (c) Concentration of dissolved $SO4^{2-}$, DOM, and H_2 in the RDI and the calculated sulfide production rate in the RDI. (d) The sulfide cycle including two production and three consumption pathways.

Then, it quickly drops to 15.7 mmol/y after 500 y and decreases further to 7.9 mmol/y after 5 ky (the slope of sulfide production in Fig. 4(d)). The rate becomes relatively stable from 5 ky to 300 ky, with very slow decreases, yielding an average production rate of 7.5 mmol/y in the first 300 ky (Phase I). There is a marked peak in the sulfide flux at about 300 ky where high sulfate coincides with decreasing attenuation by goethite (Fig. 4(b)). In Phase II, following the depletion of gypsum, sulfide production rate reduces to a stable value of 3.9 mmol/y after 450 ky, which is roughly a factor two lower than the production rate during Phase I. After about 750 ky, SOM in the lower buffer is substantially consumed, which causes a small decline in the sulfide flux and a slower increase in the max. corrosion depth at the bottom of the canister.

4.3. Sulfide attenuation – the iron system

The most important sink for the produced sulfide is the attenuation by the iron system while sulfide diffuses through the bentonite barrier. The key processes consuming sulfide are goethite dissolution accompanied by the released Fe^{2+} in the bentonite and mackinawite precipitation near the EDZ according to equations (9) and (10), respectively (Fig. 3). During Phase I, despite the higher sulfide production rate, only 1.6% of the produced sulfide reaches the canister surface at 300 ky due to strong attenuation by the iron system. Over the course of 1 My, 52% of the total produced sulfide has precipitated as mackinawite, 41% is consumed by the reaction with goethite (converted into elemental sulfur), while only 6% has reached the canister surface and caused it to corrode (Fig. 4(d)). This mass balance indicates that very little sulfide diffuses into the rock and ultimately leaves the model domain by diffusing through the boundaries. This is consistent with the nearly zero sulfide flux across the open boundaries shown in Fig. 4(a).

Furthermore, the small fraction of the sulfide reaching the canister proves the efficiency of the iron system in shielding the canister from corrosive fluxes and indicates that the produced sulfide is rapidly immobilized by incorporation into solid phases near the EDZ. Fig. 5 shows that the sulfide produced from the RTI is at all times equal to the sulfide that is consumed by the iron system in the upper part of the model (the backfilled tunnel, RTI, and the upper surrounding rock). In other words, due to the backfill barrier, there is no net flux of sulfide from the upper part of the model to the canister. In contrast, in the lower part of the model (the disposal hole, RDI, and the lower surrounding rock), the consumption of sulfide by the iron system is slightly lower than that is produced from the RDI, leading to a net sulfide flux towards the canister. The evolution of the sulfide flux to the canister surface (Fig. 4(b)) matches the differences between the produced and attenuated sulfide (Fig. 5), indicating that the sulfide reactions in the lower part of the model dominate the sulfide flux to the canister. During Phase II, goethite is nearly depleted in the mid and lower buffer (Fig. 3), leading to a significantly weakened protection of the canister and heterogeneous corrosion focusing at the bottom corner of the canister. The more steady supply of sulfate and the weaker sulfide attenuation in the lower buffer contribute to a more stable sulfide flux to the canister.

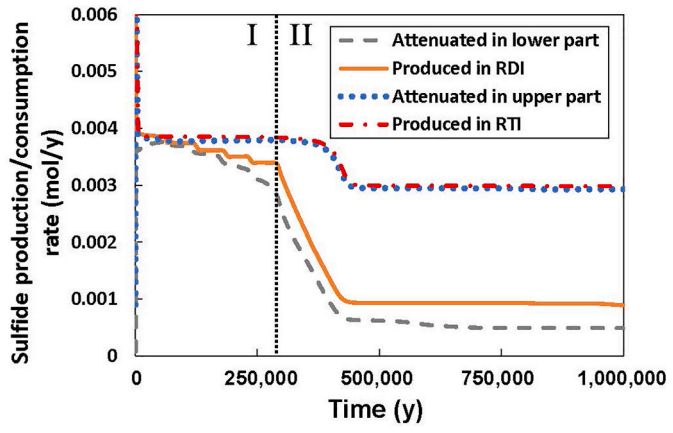

Fig. 5. Sulfide production rate in the RDI and RTI, and consumption rate by the iron system in the upper (backfill, RTI, and the upper surrounding rock) and lower (buffer, RDI and the lower surrounding rock) model.

At 1 My, 95% of the aqueous Fe^{2+} is provided by goethite dissolution in the clays, whereas only 5% comes from chamosite dissolution in the host rock (Eq. (11)). About 62% of the produced Fe^{2+} precipitates as mackinawite, about 34% precipitates as siderite in the backfill and buffer, and the remainder reacts with the clay exchanger or is lost through the open boundaries (Fig. 6).

4.4. Canister corrosion depth

The evolution of surface-averaged corrosion depth of the canister is presented in Fig. 4(b). The average corrosion rate stabilizes during Phase II at about 0.37 nm/y, due to steady sulfide production and weak sulfide attenuation in the mid and lower buffer. The maximum cell-resolved corrosion depths deviate from the average corrosion depth during Phase II (Fig. 4(b)), indicating heterogeneous corrosion rates at the canister surface during that phase. For example, the relative standard deviation of the corrosion depth on the vertical canister wall is 12.5% at 200 ky, and increases to 75.1% at 1 My (Fig. 7). As shown in Fig. 6, over the course of one million years, the top surface of the canister is well protected by the bentonite above the canister. However, the bottom of the canister is rather poorly protected, especially during the transition from Phase I to Phase II (about 200 ky - 400 ky), when the production rate of sulfide is still high, and the goethite in the bottom corner is already largely consumed. After 1 My, the average corrosion depth is predicted to be 0.26 mm, whereas the max. corrosion depth is predicted to be 1.3 mm, which is safely within the designed thickness of the copper layer of 50 mm (Jonsson et al., 2018). Highest corrosion rates occur at the canister's bottom corner, caused by the canister geometry (the corner is exposed to sulfide fluxes from the bottom and the sides) and depletion of goethite in the lower buffer.

5. Discussion

The reference model described above is developed based on current

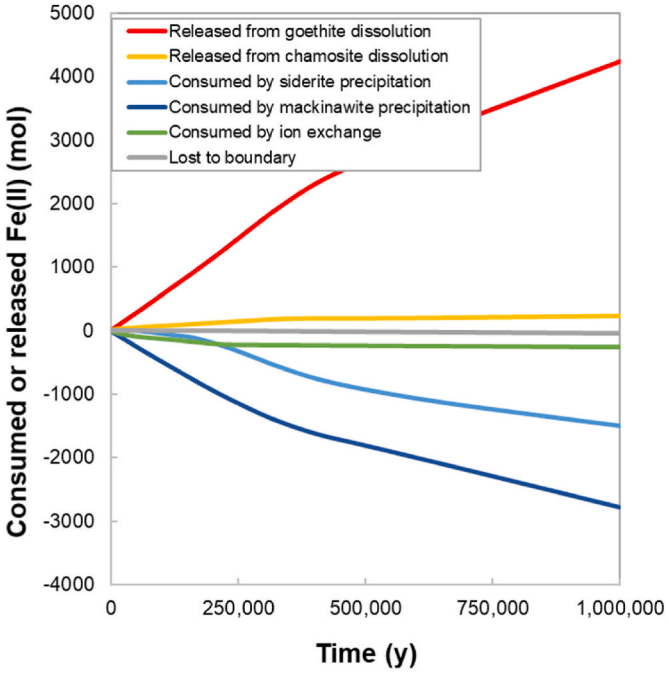

Fig. 6. Evolution of consumed and released aqueous Fe (mol) in the system.

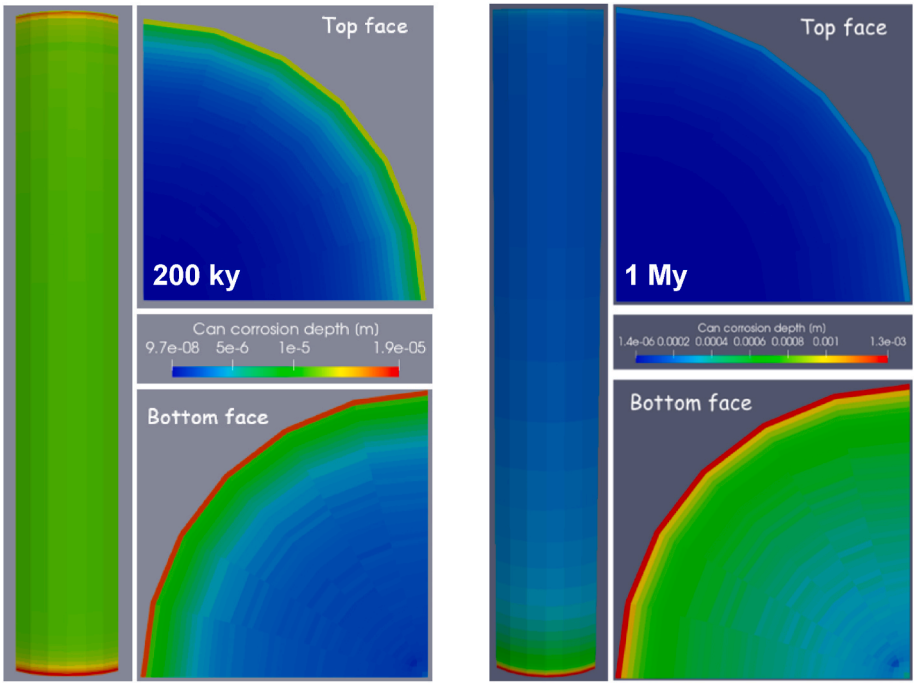

Fig. 7. Distribution of cell corrosion [m] at 200 ky (left) and 1 My (right) on the canister surface.

understanding of the near-field conditions at the Olkiluoto site. Although the model captures accurately the geometry of the repository, the processes and couplings between them, and the distribution of materials and properties, there are still uncertainties and questions related to the conceptualization and parameterization of the model.

One important outcome of the reference model is that the backfill effectively shields the canister from sulfide fluxes released from the RTI by its iron system. The question is then whether the backfill has any effect on canister corrosion and whether a simpler model of the deposition hole is sufficient to accurately predict the canister corrosion rates. Another important question is how much uncertainty there is when the ambient groundwater is represented by a fixed groundwater composition at the boundaries. Finally, the results of the simulation depend on the various parameters, such as mineral inventories, initial porewater compositions, SRB rates, etc. These questions and uncertainties in the model parameterization and the impact of some key parameters are discussed in the following sections.

5.1. Role of the backfilled tunnel

Here, we take advantage of the 3D geometry to investigate the impact the backfilled tunnel on sulfide corrosion. Fig. 5 shows that the upper model (the backfill, RTI, and upper host rock) consumes almost all the sulfide that is produced in the RTI, without affecting sulfide forming in the lower model. This indicates that the exchange of sulfide between the backfilled tunnel and the buffer is highly limited, due to the slow diffusion and the fast sulfide attenuation in the bentonites. However, the backfilled tunnel can still participate in the sulfide corrosion process by exchanging chemical constituents such as sulfate, DOM, or Fe(II). In the reference model, the initial sulfate concentration, constrained by gypsum equilibrium, is higher in the backfill porewater (Italian bentonite) than that in the buffer (Wyoming bentonite), resulting in sulfate diffusing from the backfill towards the buffer and triggering gypsum precipitation in the upper buffer in the first 10–20 ky (SI Fig. S5). This extra sulfate in the buffer enhances sulfide production at later times and leads to stronger canister corrosion compared to cases not considering the backfill. In order to acquire a better understanding of the governing processes taking place in the backfill that affect the sulfide fluxes, and to quantify the impact of the backfill tunnel on canister corrosion, a test case that does not consider the backfill is presented in the SI-Section 5.1. The comparison between this test case and the reference case demonstrates that the exchange of sulfate between the backfill and the buffer considerably increases the sulfide fluxes over the long term and contributes to about 34% of the average canister corrosion (for details, see SI-Section 5.1). However, it is important to note that, this contribution from the backfill arises from the differences in the porewater compositions between the backfill and the buffer, which could be caused by the differences in mineral and exchanger compositions, residual water contents, and the subsequent mass transport and reactions due to SRB activity. One implication is that if the same bentonite materials are used for both the backfill and the buffer (implying the same initial and equilibrium porewater composition), the impact of the backfill is expected to be negligible.

5.2. Uncertainties in the boundary conditions

One of the uncertainties of the model, which is almost inevitable in such numerical simulations, is the thickness of the surrounding rock and the impact of the choice of boundary condition on the modelling results. In this study, the groundwater composition is fixed at boundaries not constituting planes of symmetry, allowing for species diffusion across the boundaries. According to Fick's law, a thicker rock interval between repository and boundary will result in smaller concentration gradients and slower diffusion rates. Thus, in a purely diffusive system the impact of the boundary decreases when the model boundary is more extended into the rock. In terms of sulfate transport, a rock interval of infinite dimension would lead to slower sulfate out-diffusion into the rock (due to elevated sulfate concentrations in the rock) and zero sulfate loss to the boundaries when sulfate is available in excess (e.g. in Phase I of the reference model). Later, when sulfate in the near field gets depleted (e.g. in Phase II of the reference model), sulfate in the rock can eventually diffuse back towards the disposal hole to support SRB reactions. In other words, with an infinite rock interval, sulfate can be 'preserved' in the surrounding rock without leaving the system. This is similar to the idea of sulfate conservation and sulfate limited corrosion (Pekala et al., 2020) that is used in some other models. One way to achieve sulfate

conservation and to mimic the effect of an infinite rock interval is to set fully closed boundaries which traps all the sulfate inside the model. In SI-Section 5.2, a bounding case with all the boundaries closed is presented, showing that the closed boundaries significantly increase sulfate concentrations in the porewater and enhance SRB activities during the entire simulation such that Phase II has become irrelevant. Consequently, the transport of DOM becomes the only rate-limiting factor for sulfide production, which leads to much higher sulfide fluxes after 300 ky compared to the reference case (SI Fig. S8) and larger corrosion depths in the upper canister (for details, see SI-Section 5.2). Note that the assumptions that underline the scenario of fully closed boundaries are that all the sulfate 'preserved' in the rock will be available for SRB reactions, and, unlike in the reference case, sulfate will not be supplied by groundwater after the depletion of sulfate in the near field. Moreover, fully closed boundaries do not capture the accurate diffusion processes by trapping sulfate completely in the near field. Thus, the arrival of Phase II, at which point sulfate diffuses from the surrounding rock towards the disposal hole, cannot be properly predicted. On the other hand, concentration gradients between the near field and the rock are expected to be steeper when advection is a significant transport mechanism in the rock. Hence one could argue that fixing the groundwater composition along the boundaries and by this steepening the concentration gradients in the rock, mimics a situation where there is advective transport occurring in the rock at some distance from the disposal hole.

5.3. Uncertainties in mineral inventories and porewater compositions

The results of the model depend on the choice of initial conditions and system parameters. Although the repository's solid materials, their properties, and their porewaters are represented based on experimental observations and conservative judgements (Section 3.2 and 3.3), it is important to acknowledge the uncertainties in the model parameterization and their impacts on the modelling results. A series of sensitivity cases are presented in the SI Section 5.3-5.6. Due to the lack of experimental data, arbitrary values are used in the sensitivity cases as illustrative examples of the impacts of these uncertainties on the predicted canister corrosion depth. Below, the main conclusions from these sensitivity cases are discussed.

5.3.1. Availability of substrates for SRB reactions

One major uncertainty regards the availability of substrates for SRB reactions, for example, the content of reactive SOM in the bentonites, the DOM and H_2(aq) concentrations in the porewaters, and the sulfate concentrations in the groundwater. In the reference model, where all analytically determined organic material is conservatively assumed to be fully soluble, DOM is by far the dominant electron donor for the SRB reactions. However, as discussed in SI-Section 4, the leachable SOM and its solubility is still debatable. A sensitivity case presented in SI-Section 5.3 assumes that only 10% of the total SOM present in the bentonite can dissolve, while the remainder constitutes an insoluble residue. With less SOM in the clays, a significantly lower corrosion depth is calculated, due to earlier depletion of SOM. Similarly, lowering the initial DOM concentrations in the bentonite porewaters also leads to substantially less canister corrosion (SI-Fig. S12(a)). In both cases, DOM transport clearly limits the rate of SRB activity. However, a case with higher initial DOM concentration in the bentonites (for details, see SI Section 5.4) yields canister corrosion rates that are very similar to the reference values (SI-Fig. S12(b)). The extra sulfide that is produced in the early phase is quickly attenuated by the iron system. A variation in the initial H_2(aq) concentrations in the clay porewaters shows limited impact on the canister corrosion (SI-Figs. S12(c) and (d)), as only about a few percent of sulfide is produced via the H_2 pathway. The sulfate concentration in the groundwater is the rate-limiting factor for SRB reaction during Phase II. As the reference model assumes a sulfate-rich brackish groundwater, a lower sulfate concentration can lead to significantly less canister corrosion.

5.3.2. Uncertainties in the iron system

The presence of Fe(III) oxides (implemented as goethite) is the key to sulfide attenuation in the system. This is because it does not only directly react with sulfide, but also provides the majority of aqueous Fe^{2+} for mackinawite precipitation, which together consume about 94% of produced sulfide in 1 My. The reference model considers that sulfide can react with all the Fe(III) oxides present in the bentonite. In order to address the uncertainty in the available Fe(III) oxides, a pessimistic case with only 10% of the goethite in both buffer and backfill compared to the reference case is presented in SI-Section 5.5. A reduced goethite content leads to earlier exhaustion of goethite in buffer (SI Fig. S13) and significantly higher sulfide fluxes towards the canister (SI Fig. S14). In the case of 10% goethite present in the bentonite, the max. corrosion depth is about 4 times that of the reference case at 1 My. Whereas in a more extreme case of no goethite present in the bentonite, the max. corrosion depth would be as high as 20 times that of the reference case at 1 My.

Furthermore, given that there is sufficient Fe(II), mackinawite is considered to be the solubility limiting mineral for sulfide in the model. As discussed in the SI-Section 3, mackinawite could convert to pyrite, especially in the long term. Given the very low solubility of pyrite under oxygen-free conditions, sulfide concentrations controlled by equilibrium with pyrite would be orders of magnitude lower. However, this transformation reaction is very system-dependent and for conservative reasons, we do not include the transformation from mackinawite to pyrite in the model.

5.3.3. Diffusion coefficient of the rock and clay

Different regions in the model are idealized to be compartments with average porous equivalent properties based on the available information. However, due to the sparsely fractured nature of the rock, the effective diffusion coefficients of the rock as well as the EDZ are difficult to ascertain. Moreover, diffusion in the bentonites is assumed to be homogeneous, while all diffusing species have the same effective diffusion coefficient. Such a simplified formulation ignores additional processes associated with solute diffusion in compacted clays, such as species dependent diffusion and electrochemical migration related to the effect of the negative surface charge of clay minerals on ion distributions and transport. These can be more accurately described using multi-porosity models implementing diffuse double layers (e.g. Alt-Epping et al., 2018). In addition, the dependence of diffusion coefficient on temperature is not considered in the model. The increase in temperature in the near field due to the release of decay heat from the canisters can enhance diffusion by a factor of about 3 in the early stage (Wersin et al., 2014). In order to envelope these uncertainties in the diffusion process, several cases with increased or decreases effective diffusion coefficients in the rock and EDZ, or in the bentonites are presented in SI Section 5.6. The results show that increased diffusion coefficients, either in the rock or in the clay, enhance the sulfide fluxes to some extent, and likewise, decreased diffusion coefficients mildly reduce the sulfide fluxes. However, due to the buffering by the iron system and limited SOM inventory in the buffer, overall the impact of diffusion coefficients are insignificant on the canister corrosion.

6. Conclusions

This study presents a 3D reactive transport model to assess the sulfide fluxes and the spatially resolved canister corrosion depth in the KBS-3 disposal concept. The parameterization of the model is based on conservative but reasonable assumptions from experimental findings and current understanding. Simulations predict focused corrosion of the canister at the bottom corner, with a max. corrosion depth of 1.3 mm after 1 My, which is safely within the designed thickness of the copper layer (50 mm, Jonsson et al., 2018). It also demonstrates the strong impact of gypsum and SOM on sulfide production, as well as Fe(III) oxides on sulfide scavenging, which together control the net sulfide flux

reaching the copper canister. The role of H_2 as potential electron donor for SRB metabolism is negligible. Gypsum, present as accessory mineral in the buffer material, provides sufficient sulfate for SRB reactions for about 300 ky. Following the depletion of gypsum, the source of sulfate changes from near-field gypsum dissolution to a far-field source of groundwater diffusion, which leads to slower but steady sulfide production. SOM in the buffer can support SRB for nearly 1 My, and a reduced reactive SOM content effectively decreases the canister corrosion depth. During sulfide diffusion through the bentonite barriers, goethite (used as a proxy for Fe(III) oxides) plays a critical role in sulfide attenuation, because on one hand, it directly reacts with about 41% of the produced sulfide (at 1 My) inside the bentonite, and on the other hand it provides about 95% of Fe(II) available for mackinawite precipitation near the EDZ, which consumes about 52% of the sulfide at 1My. It is important to note that pyrite formation has not been considered in the model. The transformation of mackinawite, a fairly soluble phase, to pyrite would lead to much lower sulfide concentrations and fluxes. Due to strong sulfide-attenuation by Fe(III) oxides in the backfilled tunnel, the backfill material does not directly affect sulfide fluxes to the canister. This implies that the mineral inventories in the buffer dominates the evolution of the sulfide flux to the canister. Simulations show that corrosion rates cannot be predicted solely based on the inventory of electron donors and acceptors in the repository, but they are a result of multiple interacting transport and reaction processes that vary in space and time. The complexity of the system is indicated by a spatially heterogeneous distribution of corrosion depths on the canister surface after 1 My, emphasizing the importance of using realistic 3D geometries of the near field in model simulations. It is important to point out that there are still considerable uncertainties in the model parameterization. The most important uncertainties regard the availability of organic carbon and the interaction between sulfide and Fe(III) phases. Further studies gaining understanding of these processes can certainly be helpful to improve the model.

Declaration of competing interest

The authors declare the following financial interests/personal relationships which may be considered as potential competing interests:

Jin Ma, Paul Wersin reports financial support was provided by Posiva Oy.

Data availability

Data will be made available on request.

Acknowledgements

Financial support by Posiva Oy is acknowledged. The model development has been carried within Posiva's Safety Case for the Operating Licence Application (SC-OLA).

Appendix A. Supplementary data

Supplementary data to this article can be found online at https://doi.org/10.1016/j.apgeochem.2022.105439.

References

Aaltonen, I., Front, K., Gehör, S., Sahlstedt, E., 2018. Hydrothermal Alteration of Bedrock at Olkiluoto. Posiva Report 2018-03. Posiva Oy, Olkiluoto, Eurajoki, Finland.

Alt-Epping, P., Wersin, P., 2018a. Reactive Transport Modelling of Sulfide Fluxes in the Near-Field: Summary of Mdoel Development and Application to a Simplified Backfill-Buffer-Rock System in 2014 and 2015. Posiva Working Report WR 2017-50.

Alt-Epping, P., Gimmi, T., Wersin, P., Jenni, A., 2018. Incorporating electrical double layers into reactive-transport simulations of processes in clays by using the Nernst-Planck equation: a benchmark revisited. Appl. Geochem. 89, 1–10.

Bagnoud, A., Chourey, K., Hettich, R.L., De Bruijn, I., Andersson, A.F., Leupin, O.X., Schwyn, B., Bernier-Latmani, R., 2016. Reconstructing a hydrogen-driven microbial metabolic network in Opalinus Clay rock. Nat. Commun. 7, 1–10. https://doi.org/10.1038/ncomms12770.

Bradbury, M.H., Baeyens, B., 1997. A mechanistic description of Ni and Zn sorption on Na-montmorillonite Part II: modelling. J. Contam. Hydrol. 27, 223–248.

Bradbury, M.H., Baeyens, B., 2002. Porewater Chemistry in Compacted Re-saturated MX-80 Bentonite: Physico-Chemical Characterisation and Geochemical Modelling. Nagra Technical Report NTB 01-08. Wettingen, Switzerland.

Bradbury, M.H., Baeyens, B., 2003. Porewater chemistry in compacted re-saturated MX-80 bentonite. J. Contam. Hydrol. 61, 329–338.

Briggs, S., McKelvie, J., Keech, P., Sleep, B., Krol, M., 2016. Transient modelling of sulfide diffusion under conditions typical of a deep geological repository. Corrosion Eng. Sci. Technol. 52 (Suppl. 1), 200–203.

Charlet, L., Tournassat, Ch, 2005. Fe(II)–Na(I)–Ca(II) cation exchange on montmorillonite in chloride medium: evidence for preferential clay adsorption of chloride – metal ion pairs in seawater. Aquat. Geochem. 11, 115–137.

Cloet, V., Pekala, M., Smith, P., Wersin, P., Diomidis, N., 2017. An Evaluation of Sulfide Fluxes in the Near Field of a HLW Repository. Nagra Technical Report NTB 17-04. Wettingen, Switzerland.

Dos Santos Afonso, M., Stumm, W., 1992. Reductive dissolution of iron (iii)(hydr) oxides by hydrogen sulfide. Langmuir 8, 1671–1675.

Fox, A., Forchhammer, K., Pettersson, A., La Pointe, P., Lim, D.H., 2012. Geological Discrete Fracture Network Model for the Olkiluoto Site. Eurajoki, Finland. Version 2.0.

Goldhaber, M.B., Kaplan, I.R., 1975. Controls and consequences of sulfate reduction rates in recent marine sediments. Soil Sci. 119, 42–55.

Hartley, L., Appleyard, P., Baxter, S., Hoek, J., Roberts, D., Swan, D., 2013. Development of a Hydrogeological Discrete Fracture Network Model for the Olkiluoto Site Descriptive Model 2011. Working Report 2012-32. POSIVA OY.

Hellä, P., Pitkänen, P., Löfman, J., Partamies, S., Vuorinem, U., Wersin, P., 2014. Safety Case for the Disposal of Spent Nuclear Fuel at Olkiluoto. Definition of Reference and Bounding Groundwaters, Buffer and Backfill Porewaters. POSIVA 2014-04. POSIVA OY.

Jonsson, M., Emilsson, G., Emilsson, L., 2018. Mechanical Design Analysis for the Canister. Posiva SKB Report 04, 2489-2742.

Jin, Q., Roden, E.E., Giska, J.R., 2013. Geomicrobial kinetics: extrapolating laboratory studies to natural environments. Geomicrobiol. J. 30, 173–185. https://doi.org/10.1080/01490451.2011.653084.

Karnland, O., Olsson, S., Nilsson, U., 2006. Mineralogy and Sealing Properties of Various Bentonites and Smectite-Rich Clay Materials. SKB Technical Report TR-06-30.

Kiczka, M., Pekala, M., Wersin, P., 2020. Radionuclide Solubility Limits and Migration Parameters for the Canister, Buffer and Buffer-Rock Interface for SC-OLA Part II - Migration Parameters. Posiva Working Report WR 2022-03. Olkiluoto, Eurajoki, Finland.

Kiczka, M., Pekala, M., Maanoja, S., Muuri, E., Wersin, P., 2021. Modelling of solute transport and microbial activity in diffusion cells simulating a bentonite barrier of a spent nuclear fuel repository. Appl. Clay Sci. 211, 106193.

King, F., Chen, J., Qin, Z., Shoesmith, D., Lilja, C., 2017. Sulphide-transport control of the corrosion of copper canisters. Corrosion Eng. Sci. Technol. 52 (Suppl. 1), 210–216.

King, F., Kolář, M., Puigdomenech, I., Pitkänen, P., Lilja, C., 2020. Modeling microbial sulfate reduction and the consequences for corrosion of copper canisters. Mater. Corros. 72, 339–347.

Kiviranta, L., Kumpulainen, S., Pintado, X., Kartuunen, P., Schatz, T., 2018. Characterization of Bentonite and Clay Materials 2012-2015. Posiva Working Report WR 2016-05.

Maanoja, S., Lakaniemi, A.-M., Lehtinen, L., Salminen, L., Auvinen, H., Kokko, M., Palmroth, M., Muuri, E., Rintala, J., 2020. Compacted bentonite as a source of substrates for sulfate-reducing microorganisms in a simulated excavation-damaged zone of a spent nuclear fuel repository. Appl. Clay Sci. 196, 105746.

Maanoja, S., Palmroth, M., Salminen, L., Lehtinen, L., Kokko, M., Lakaniemi, A.M., Auvinen, H., Kiczka, M., Muuri, E., Rintala, J., 2021. The effect of compaction and microbial activity on the quantity and release rate of water-soluble organic matter from bentonites. Appl. Clay Sci. 211, 106192.

Maia, F., Puigdomenech, I., Molinero, J., 2016. Modelling Rates of Bacterial Sulfide Production Using Lactate and Hydrogen as Energy Sources. SKB TR-16-05. Swedish Nuclear Fuel and Waste Management Co, Stockholm, Sweden.

Masurat, P., Eriksson, S., Pedersen, K., 2010. Microbial sulfide production in compacted Wyoming bentonite MX-80 under in situ conditions relevant to a repository for high-level radioactive waste. Appl. Clay Sci. 47, 58–64.

Mäkelä, J., Mäkelä, M., Koikkalainen, K., Manninen, P., 2016. Study of Humic Substances and Dissolved Organic Matter Isolated from the Goundwater of ONKALO, Olkiluoto, 2014. Posiva Working Report 2016-03.

Nethe-Jaenchen, R., Thauer, R.K., 1984. Growth yields and saturation constant of Desulfovibrio vulgaris in chemostat culture. Arch. Microbiol. 137, 236–240.

Pekala, M., Wersin, P., Cloet, V., Diomidis, N., 2019a. Reactive transport calculations to evaluate sulphide fluxes in the near-field of a SF/HLW repository in the Opalinus Clay. Appl. Geochem. 100, 169–180. https://doi.org/10.1016/j.apgeochem.2018.11.006. October 2018.

Pekala, M., Alt-Epping, P., Wersin, P., 2019b. 3D and 1D dual-porosity reactive transport simulations - model improvements, sensitivity analyses, and results from the integrated sulfide project inter-model comparison exercise. Posiva Work. Rep. 2018–2031.

Pekala, M., Smith, P., Wersin, P., Diomidis, N., Cloet, V., 2020. Comparison of models to evaluate microbial sulphide generation and transport in the near field of a SF/HLW repository in Opalinus Clay. J. Contam. Hydrol. 228, 103561.

Pedersen, K., Motamedi, M., Karnland, O., Sandén, T., 2000. Mixing and sulphate-reducing activity of bacteria in swelling, compacted bentonite clay under high-level radioactive waste repository conditions. J. Appl. Microbiol. 89, 1038–1047.

Pedersen, K., Bengtsson, A., Blom, A., Johansson, L., Taborowski, T., 2017. Mobility and reactivity of sulphide in bentonite clays–implications for engineered bentonite barriers in geological repositories for radioactive wastes. Appl. Clay Sci. 146, 495–502.

Posiva, 2021. Sulfide Fluxes and Concentrations in the Spent Nuclear Fuel Repository at Olkiluoto - 2021 Update. Posiva Working Report 2021-07.

Poulton, S.W., Krom, M.D., Raiswell, R., 2004. A revised scheme for the reactivity of iron (oxyhydr)oxide minerals towards dissolved sulfide. Geochem. Cosmochim. Acta 68, 3703–3715.

Richards, C., Pallud, C., 2016. Kinetics of sulfate reduction and sulfide precipitation rates in sediments of a bar-built estuary (Pescadero, California). Water Res. 94, 86–102.

Rickard, D., Luther, G.W., 2007. Chemistry of iron sulfides. In: Chemical Reviews. https://doi.org/10.1021/cr0503658, 107, Issue 2.

Salonen, T., Lamminmäki, T., King, F., Pastina, B., 2021. Status report of the Finnish spent fuel geologic repository programme and ongoing corrosion studies. Mater. Corros. 72 (1–2), 14–24. https://doi.org/10.1002/maco.202011805.

Smith, J., Qin, Z., King, F., Werme, L., Shoesmith, D.W., 2007. Sulfide film formation on copper under electrochemical and natural corrosion conditions. Corrosion 63 (2), 135–144.

Stenlid, J.H., Dos Santos, E.C., Bagger, A., Johansson, A.J., Rossmeisl, J., Pettersson, L.G., 2019. Electrochemical interface during corrosion of copper in anoxic sulfide-containing groundwater—a computational study. J. Phys. Chem. C 124 (1), 469–481.

Stone, W., Kroukamp, O., McKelvie, J., Korber, D.R., Wolfaardt, G.M., 2016. Microbial metabolism in bentonite clay: saturation, desiccation and relative humidity. Appl. Clay Sci. 129, 54–64.

Stroes-Gascoyne, S., Hamon, C.J., Maak, P., Russell, S., 2010. The effects of the physical properties of highly compacted smectitic clay (bentonite) on the culturability of indigenous microorganisms. Appl. Clay Sci. 47, 155–162.

Svensson, D., Lundgren, C., Wikberg, P., 2017. Experiments with Bentonite and Sulfide – Results from Experiments 2013–2016. SKB Report P-16-31. Stockholm, Sweden.

Wersin, P., Leupin, O.X., Mettler, S., Gaucher, E.C., Mäder, U., De Cannière, P., Vinsot, A., Gäbler, H.E., Kunimaro, T., Kiho, K., Eichinger, L., 2011. Biogeochemical processes in a clay formation in situ experiment: Part A - overview, experimental design and water data of an experiment in the Opalinus Clay at the Mont Terri Underground Research Laboratory, Switzerland. Appl. Geochem. 26 (6), 931–953. https://doi.org/10.1016/j.apgeochem.2011.03.004.

Wersin, P., Pitkänen, P., Alt-Epping, P., Román-Ross, G., Smith, P., Snellman, M., Trinchero, P., Molinero, J., Filby, A., Kiczka, M., 2014. Sulfide Fluxes and Concentrations in the Spent Nuclear Fuel Repository at Olkiluoto. Report POSIVA 2014-01. Olkiluoto, Finland.

Wersin, Paul, Kiczka, Mirjam, Koskinen, Kari, 2016. Porewater chemistry in compacted bentonite: Application to the engineered buffer barrier at the Olkiluoto site. Appl. Geochem. 74, 165–175.

Wersin, Paul, Alt-Epping, Peter, Pekala, Marek, Pitkänen, Petteri, Snellman, Margit, 2017. Modelling sulfide fluxes and Cu canister corrosion rates in the engineered barrier system of a spent fuel repository. Procedia Earth. Planetary Sci. 17, 722–725.